*American Mineralogist, Volume 66, pages 507–525, 1981*

# Mineralogy and petrology of parts of the Marra Mamba Iron Formation, Hamersley Basin, Western Australia

CORNELIS KLEIN AND MARTIN J. GOLE[1]

*Department of Geology, Indiana University*
*Bloomington, Indiana 47405*

**Abstract**

The Marra Mamba Iron Formation, of early Proterozoic age (probably about 2.5 G.y.), is the lowermost member of the Hamersley Group of Western Australia. It shows well-developed mesobanding and abundant fine-scale laminations. This study characterizes the bulk chemistry, mineralogy and petrology of two distinctly different units within the iron-formation. The uppermost part consists of magnetite-rich associations which include: quartz, magnetite, minnesotaite, riebeckite, stilpnomelane, dolomite (or ankerite), calcite, and traces of pyrite. The lowermost part is sulfide-rich and contains variable amounts of: quartz, siderite, dolomite (or ankerite), stilpnomelane, minnesotaite, pyrrhotite and/or pyrite, and small amounts of carbon. Quartz is commonly microcrystalline, but the carbonates and magnetite are sub- to euhedral and medium- to coarse-grained, the result of recrystallization. Stilpnomelane and pyrite are also considerably coarser grained than quartz. Fibrous minnesotaite commonly cuts across carbonates and stilpnomelane reflecting its origin during late diagenesis or very low grade metamorphism of the assemblages. Petrologic studies in closely associated, underlying volcanics (of the Fortescue Group) reflect a range of burial metamorphic conditions within the prehnite–pumpellyite facies. The iron-formation assemblages, at very low temperatures of metamorphism, do not appear to be as sensitive to relatively small temperature changes as do very low grade metamorphic volcanics. The iron-formation assemblages may have originated over a temperature range of 100 to a maximum of about 300°C.

## Introduction and geologic setting

The Marra Mamba Iron Formation is the lowermost unit of the Proterozoic Hamersley Group in the northwestern part of Western Australia (see Fig. 1). Its areal distribution is shown in Figure 2. It conformably overlies the Roy Hill Shale Member of the Jeerinah Formation and is overlain by the Wittenoom Dolomite. The age of the iron-formations in the Hamersley Basin has been determined to be about 2.5 G.y. (Compston *et al.*, in preparation).

The Marra Mamba Iron Formation varies considerably in thickness, as based on sections measured in the field; however, not enough drill hole data are available to provide a quantitative assessment of its thickness variation throughout the Hamersley Range. Trendall and Blockley (1970) report a thickness range of 183 to 229 m based on sections measured in the western part of the Hamersley Range (see Fig. 2). Others report thicknesses that range from a minimum of 15 m (Kriewaldt and Ryan, 1967) to 183 m (MacLeod, 1966) for sections in different parts of the Hamersley Range.

The Marra Mamba Iron Formation is underlain by the Jeerinah Formation which is the uppermost member of the Fortescue Group. This group may be as much as 3660 to 4270 m thick (Trendall and Blockley 1970, and MacLeod, 1966) and consists of shales and cherts in the upper part (Jeerinah Formation), of basaltic lavas and pyroclastics in the middle part (Mt. Jope volcanics), and of sandstones, conglomerates and basic lava flows in the lower part (Hardey Sandstone). The Fortescue Group is the basal unit of the Proterozoic sequence and unconformably overlies the Archean basement (see Fig. 1).

The Marra Mamba Iron Formation has been informally subdivided into three parts (Trendall and Blockley, 1970). These are 1) the lower banded iron-formation member of about 137 m thickness, 2) the

[1] Present address: Department of Geology, Georgia State University, Atlanta, Georgia 30303.

0003–004X/81/0506–0507$02.00

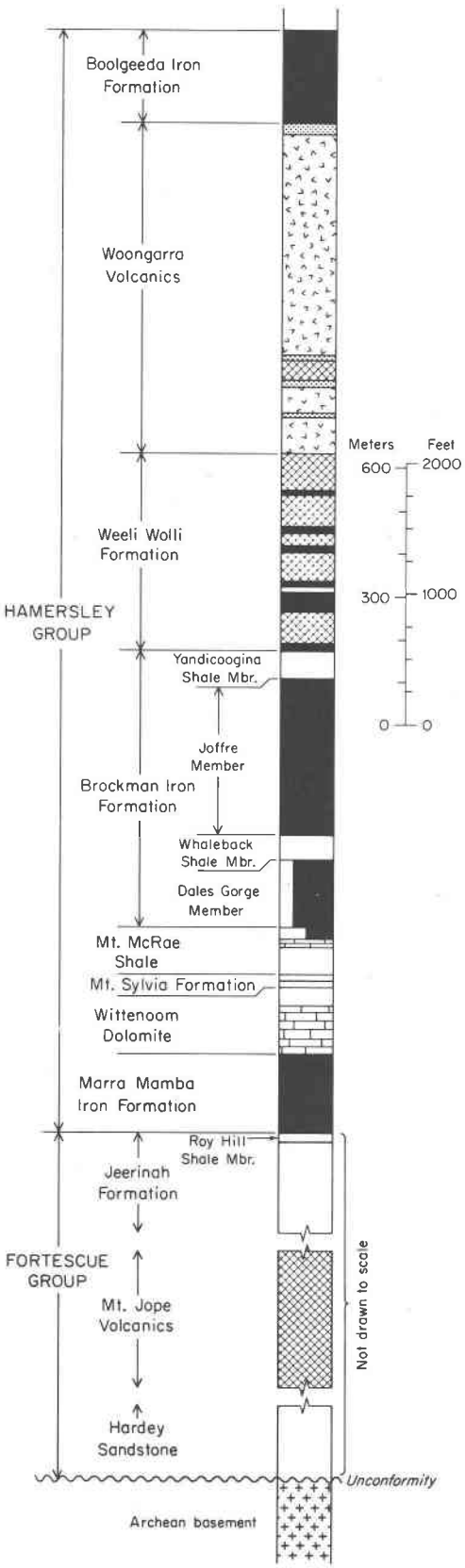


middle "shaly" member with a thickness of about 37 m, and 3) an upper banded iron-formation member of about 61 m thickness.

On account of the pervasive lateritic weathering in much of Western Australia and the generally poor outcrop of the Marra Mamba Formation, a study such as this must be based on carefully selected, unaltered material from diamond drill cores. Two diamond drill cores which partly transect the Marra Mamba Iron Formaiton were sampled for this study. The drill cores were made available by the Hamersley Exploration Pty. Limited in Wittenoom, W.A. (for location, see Fig. 2). One hole, D.D.H. no. 270, located 38 km west of Wittenoom, is 201 m deep, of which the upper 167 m consist of Wittenoom Dolomite and the remaining 34 m of the upper part of the Marra Mamba Iron Formation. This section contains fresh, unaltered iron-formation. The other hole, D.D.H. no. 182, also from the Wittenoom region, is 195 m deep of which the upper 172.5 m transects the Marra Mamba Iron Formation and the remaining 22 m the upper part of the underlying Jeerinah Formation. The upper 107 m of the Marra Mamba in this hole are heavily weathered, but the remainder of the core is fresh. This study is based on samples from the uppermost 34 m and the lowermost 65.5 m of the Marra Mamba Iron Formation and the upper 22.5 m of the underlying Jeerinah Formation.

The banded iron-formations of the Hamersley Basin have been studied in great detail with respect to their stratigraphy, chemical composition, and sedimentary and diagenetic structural features (*e.g.*, Trendall and Blockley, 1970). It is the purpose of this study to characterize the various assemblages and the compositions of the individual minerals, and to evaluate the possible metamorphic history of the lowermost unit of the iron-formations.

## Methods of study

Materials were selected from the two diamond drill cores on the basis of their apparent freshness, their diversity of mineral assemblages as reflected by pronounced color banding, and on the basis of textural variations, such as changes in mesobanding or microbanding, and grain size. Nine rock samples of the Marra Mamba Iron Formation and three of the Jeerinah Formation were analyzed by a combination

Fig. 1. Stratigraphic column of the Hamersley Group in the central part of the Hamersley Basin (after Trendall and Blockley, 1970). The approximate stratigraphy of the underlying Fortescue Group is after MacLeod, 1966.

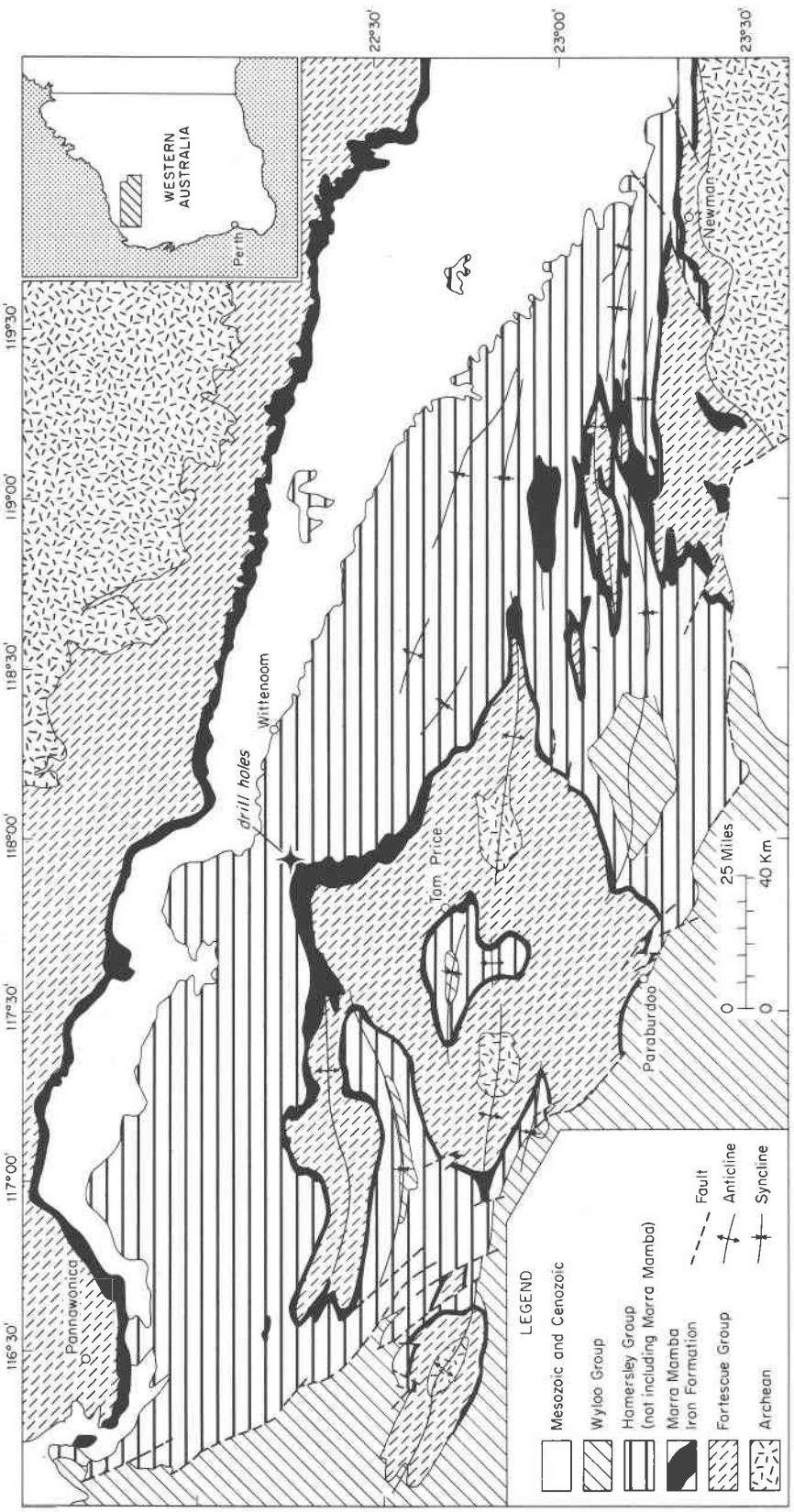


Fig. 2. Distribution of the Marra Mamba Iron Formation in the Hamersley Range (after MacLeod, 1966). The location of the two drill holes, DDH no. 182 and 270 is shown. They are approximately 4.5 km apart.

of gravimetric, flame photometric, and colorimetric techniques. Approximately 170 thin and polished thin sections were used for detailed petrographic study of the mineral assemblages and their textural relations prior to electron probe microanalysis. Chemical analyses for nine oxide components in silicates, carbonates and oxides were performed on 80 polished thin (1″ diameter) sections using a 3-spectrometer Etec Autoprobe. Approximately one thousand mineral grains were analyzed in this manner. Operating conditions and analytical procedures are outlined by Klein (1974).

### Bulk chemical analyses

Chemical analyses for twelve rock samples, each including several bands of different mineral composition, are given in weight percentage in Table 1. Nine of these are of the Marra Mamba Iron Formation and three of the immediately underlying Jeerinah Formation. Each analysis represents the average composition of a quartered section of diamond drill core with a length of about 12.5 cm. Samples 1 through 4 are from the upper part of the Marra Mamba Iron Formation in D.D.H. no. 270 (field numbers are preceded by a B); samples 6 through 10 are from the lower part of the Marra Mamba Iron Formation in D.D.H. no. 282 (field numbers are preceded by an A), which directly overlies the Jeerinah Formation; and samples 11 through 13 are from the Roy Hill Shale Member in the upper part of the Jeerinah Formation. The total Fe content of the nine samples of the Marra Mamba Iron Formation ranges from 18.05 to 44.40 percent. Samples 10 and 12 of the Roy Hill Shale Member of the Jeerinah Formation are sulfide-rich and shale-like (high $Al_2O_3$ and $K_2O$, but low total Fe), but sample 11 represents a carbonate-rich iron-formation band within the Jerrinah Formation. Samples 1 to 4 contain considerable amounts of magnetite (see assemblage listings in the footnote to Table 1) whereas samples 6 to 10 and 12 generally contain no magnetite (or only a trace) but show considerable pyrite and/or pyrrhotite contents. Such assemblage differences are clearly reflected in the $Fe^{3+}/(Fe^{2+} + Fe^{3+})$ ratios of the bulk analyses. The average of the four magnetite-rich samples can be compared with analysis no. 5 which is an average obtained by Ewers and Morris (1980) from 15 composite samples of BIF sections in the same DDH #270 core. Although their average sample is truly representative of the average bulk chemistry of part of the Marra Mamba Formation, our average of four selected sections is remarkably close to their results.

The variable $Al_2O_3$ contents and their considerable range, 0 to 5.29% (sample no. 8) for the Marra Mamba samples are a reflection of their variable stilpnomelane contents. In samples 11 and 13 the much higher $Al_2O_3$ contents reflect the abundant presence of K-feldspar, chlorite and muscovite. The MgO contents of the iron-formations show a relatively restricted range, 1.96 to 7.39 percent. CaO is highly variable, 0 to 9.41 percent, and its variations are sympathetic with the $CO_2$ content of the samples, as carbonates are the only minerals in which Ca occurs. $Na_2O$ and $K_2O$ occur both in relatively small amounts (maximum $Na_2O$ is 0.83 and maximum $K_2O$ is 1.05 percent). $Na_2O$ occurs mainly in riebeckite but is also a lesser component of stilpnomelane which is the host for all of the $K_2O$ in feldspar-free assemblages. $K_2O$ is very high in the two samples of the Jeerinah Formation on account of their abundant K-feldspar and muscovite. Sulfur is present in variable amounts in the Marra Mamba Iron Formation samples, reflecting the presence or absence of pyrite and/or pyrrhotite. Carbon is present in a graphite-like form which was identified as such only in the most C-rich samples by reflected light microscopy. Large amounts of sulfur and carbon are present in the Jeerinah Formation samples. In these, the sulfur occurs in medium- to coarse-grained pyrite- and pyrrhotite-rich bands. Abundant, very fine-grained carbon in these samples makes the fine-grained silicate host almost opaque in thin section.

### Chemical variation in mineral compositions

Of the major rock-forming minerals in the Marra Mamba Iron Formation, quartz and magnetite show no compositional deviations from the established pure end-member formulas, $SiO_2$ and $Fe_3O_4$, respectively. Pyrrhotite, pyrite, and chalcopyrite, as well as ilmenite, which sporadically occurs in trace amounts in very stilpnomelane-rich assemblages, were not analyzed in sufficient numbers to establish compositional ranges, if indeed such are present. The carbonates, stilpnomelane, and minnesotaite show considerable solid solution, and riebeckite, and greenalite, and chlorite show limited compositional variations. The extent of these substitutions will be discussed in the following section.

### Carbonates

In the assemblages of the upper part of the Marra Mamba Formation (B samples in Table 1), calcite and members of the dolomite–ankerite series are

Table 1. Chemical analyses of four samples of the upper part (nos. 1–4), and five of the lower part (nos. 6–10) of the Marra Mamba Iron Formation. Averages for these distinctly different parts are shown. Analysis no. 5 is based on 15 composite samples of BIF sections in the magnetite-rich part of D.D.H. no. 270, from Ewers and Morris, 1980. Three analyses of the underlying Jeerinah Formation are also given. Column no. 12 represents an Fe-rich band in the Jeerinah Formation (see assemblage listing in footnote).

| | Marra Mamba Iron Formation | | | | | | | | | | | | Jeerinah Formation | | |
|---|---|---|---|---|---|---|---|---|---|---|---|---|---|---|---|
| | DDH 270 | | | | | | DDH 182 | | | | | | | | |
| | 1 | 2 | 3 | 4 | Avg. 1-4 | 5 | 6 | 7 | 8 | 9 | 10 | Avg. 6-10 | 11 | 12 | 13 |
| $SiO_2$ | 45.3 | 54.0 | 44.9 | 25.6 | 42.45 | 47.49 | 37.1 | 61.3 | 41.1 | 27.9 | 62.1 | 45.9 | 54.0 | 51.7 | 47.4 |
| $TiO_2$ | 0.79 | n.d.* | 0.024 | n.d.* | 0.20 | 0.010 | 0.031 | 0.104 | n.d.* | 0.31 | 0.14 | 0.12 | 0.048 | 0.070 | 0.045 |
| $Al_2O_3$ | n.d.* | 0.32 | 0.43 | 0.86 | 0.40 | 0.25 | 2.03 | 0.69 | 5.29 | 2.55 | 0.59 | 2.23 | 17.9 | 0.86 | 16.0 |
| $Fe_2O_3$ | 14.7 | 13.1 | 24.5 | 37.7 | 22.50 | 35.93+ | 4.58 | n.d.* | 4.43 | 6.44 | 1.57 | 3.40 | n.d.* | 0.91 | 0.78 |
| FeO | 13.3 | 12.5 | 18.5 | 23.2 | 16.87 | | 32.3 | 29.4 | 25.9 | 26.6 | 21.8 | 27.2 | 7.02 | 16.40 | 9.76 |
| MnO | 0.15 | 0.14 | 0.12 | 0.058 | 0.12 | 0.136 | 0.086 | 0.029 | 0.13 | 0.28 | 0.054 | 0.12 | 0.013 | 0.35 | 0.12 |
| MgO | 5.20 | 1.96 | 3.41 | 4.57 | 3.78 | 3.36 | 3.80 | 3.70 | 7.39 | 7.32 | 2.52 | 4.95 | 1.83 | 5.17 | 1.75 |
| CaO | 9.41 | 8.44 | 2.75 | 2.65 | 5.81 | 5.52 | 0.70 | n.d.* | n.d.* | 3.82 | 2.78 | 1.46 | 0.092 | 5.13 | 1.38 |
| $Na_2O$ | 0.63 | 0.83 | 0.11 | 0.14 | 0.43 | 0.237 | 0.14 | 0.008 | 0.64 | 0.44 | 0.057 | 0.26 | 0.040 | 0.047 | 0.080 |
| $K_2O$ | 0.15 | 0.09 | 0.23 | 0.15 | 0.15 | 0.132 | 0.56 | 0.19 | 1.05 | 0.68 | 0.24 | 0.54 | 8.80 | 0.14 | 7.50 |
| $H_2O(+)$ | 1.52 | 1.12 | 1.44 | 1.12 | 1.30 | | 2.24 | 4.26 | 4.96 | 2.99 | 3.45 | 3.58 | 1.96 | 0.55 | 1.51 |
| $H_2O(-)$ | 0.24 | 0.07 | 0.23 | 0.13 | 0.17 | | 0.80 | 0.08 | 3.19 | 2.00 | 0.23 | 1.26 | 0.17 | 0.29 | 0.18 |
| $P_2O_5$ | 0.079 | 0.030 | 0.11 | 0.16 | 0.095 | 0.072 | 0.065 | 0.020 | 0.043 | 0.077 | 0.041 | 0.049 | 0.064 | 0.031 | 0.091 |
| $CO_2$ | 7.90 | 6.80 | 3.45 | 2.85 | 5.25 | 6.04 | 14.0 | 0.11 | 3.65 | 17.0 | 3.90 | 7.73 | n.d.* | 17.4 | 1.35 |
| S | 0.076 | 0.13 | 0.028 | 0.13 | 0.09 | 0.085 | 1.75 | 0.009 | 0.50 | 0.029 | n.d.* | 0.47 | 5.05 | 0.45 | 8.66 |
| C | 0.09 | 0.02 | 0.17 | 0.17 | 0.11 | ____ | 0.13 | n.d.* | 1.74 | 1.28 | 0.21 | 0.67 | 3.28 | 0.36 | 3.57 |
| Total | 99.53 | 99.55 | 100.40 | 99.49 | 99.73 | 99.17+ | 100.31 | 99.90 | 100.01 | 99.72 | 99.68 | 99.94 | 100.27 | 99.86 | 100.18 |
| Total Fe | 20.62 | 18.88 | 31.52 | 44.40 | 28.85 | 25.13 | 28.31 | 22.85 | 23.23 | 25.18 | 18.05 | 23.52 | 5.46 | 13.39 | 8.14 |
| $\frac{Fe^{3+}}{(Fe^{2+}+Fe^{3+})}$ | 0.50 | 0.49 | 0.54 | 0.59 | 0.55 | | 0.11 | 0 | 0.13 | 0.18 | 0.06 | 0.10 | 0 | 0.05 | 0.07 |
| *Field #* | *B3* | *B5* | *B8* | *B12* | | | *A7* | *A16* | *A37* | *A42* | *A48* | | *A54* | *A58* | *A61* |
| Depth (meters) | 176.0 | 181.4 | 185.0 | 189.0 | | | 113.4 | 129.3 | 152.1 | 154.6 | 164.4 | | 175.1 | 186.3 | 192.5 |

*n.d.* = none detected; M. E. Coller, analyst for all analyses of this study; + all Fe recalculated as $Fe_2O_3$; † includes loss on ignition = 5.66 o/o.*

*Assemblages (minerals listed in decreasing order of abundance; those in trace amounts are in parentheses) 1: qtz-mag-rieb-dol(to ank)-cal-stilp-(tc); 2: qtz-mag-rieb-stilp-ank(to dol)-cal-minn-(py); 3: qtz-mag-dol(some ank)-stilp-rieb-minn; 4: mag-qtz-dol-rieb-stilp-tc-(py); 5: average for 15 BIF subdivisions of the Marra Mamba (Ewers and Morris, 1980); 6: stilp-sid-py-minn-(mag and po in py); 7: minn-qtz; 8: stilp-rip-dol-po-carbon-(ilm)-(cp); 9: dol-stilp-sid-carbon-(po)-(ilm); 10: qtz-minn-ank-stilp-(carbon)-(po)-(ilm); 11: Kspar-qtz-chl-py-musc-carbon-(po+cp)-(carb); 12: dol-sid-stilp-qtz-po-carbon; 13: qtz-Kspar-musc-py-carbon-carb-chl-(cp). Assemblages 11 and 13 are extremely fine-grained except for the sulfides; their silicates were identified by x-ray diffractometer.*

*Mineral abbreviations used throughout:*

*ank = ankerite*
*cal = calcite*
*carb = carbonate*
*carbon = carbonaceous (graphitic) material*
*chlor = chlorite*
*cp = chalcopyrite*
*dol = dolomite*
*green = greenalite*
*ilm = ilmenite*
*Kspar = potassium feldspar*
*minn = minnesotaite*
*musc = muscovite*
*po = pyrrhotite*
*py = pyrite*
*qtz = quartz*
*rieb = riebeckite*
*rip = ripidolite*
*sid = siderite*
*stilp = stilpnomelane*
*tc = talc*

commonly major constituents. Pairs of coexisting calcite and dolomite (or ankerite) are also abundant. Such carbonates tend to be medium- to coarse-grained, commonly with almost euhedral outlines, reflecting considerable recrystallization. The carbonate grains may form relatively continuous, thin bands between bands of magnetite or Fe-silicates, or they may be irregularly distributed among silicate–magnetite–carbonate assemblages. Representative electron microprobe analyses showing the range of calcite compositions encountered in this study are given in Table 2; Figure 3a shows their complete compositional range graphically.

Members of the dolomite–ankerite series occur in most of the Marra Mamba samples but dolomite (or ankerite)–calcite pairs occur only in the upper part of the Marra Mamba Formation (B samples in Tables; Figure 3a) and dolomite (or ankerite)–siderite pairs only in the lower (sulfide-rich and magnetite-free) part of the Formation (A samples in Tables; Figure 3b). The compositional range of the very abundant members of the dolomite–ankerite series is shown by

Table 2. Representative electron probe analyses of calcite in the Marra Mamba Iron Formation.

| | 1* | 2 | 3 | 4* | 5 | 6 | 7 | 8 |
|---|---|---|---|---|---|---|---|---|
| FeO | 0.94 | 0.97 | 1.00 | 1.08 | 1.38 | 1.53 | 1.65 | 2.03 |
| MnO | 0.25 | 0.99 | 1.14 | 0.42 | 1.01 | 0.43 | 1.86 | 0.41 |
| MgO | 0.24 | 0.49 | 0.42 | 0.51 | 0.56 | 0.49 | 0.67 | 0.47 |
| CaO | 53.02 | 54.03 | 55.49 | 54.41 | 53.46 | 55.88 | 52.45 | 52.27 |
| TOTAL | 54.45 | 55.73 | 58.05 | 56.42 | 56.41 | 58.33 | 56.63 | 55.18 |
| | recalculated on the basis of 2(Fe,Mn,Mg,Ca) | | | | | | | |
| Fe | 0.027 | 0.027 | 0.028 | 0.030 | 0.039 | 0.041 | 0.046 | 0.058 |
| Mn | 0.007 | 0.028 | 0.032 | 0.012 | 0.029 | 0.012 | 0.052 | 0.012 |
| Mg | 0.012 | 0.024 | 0.021 | 0.025 | 0.028 | 0.023 | 0.033 | 0.024 |
| Ca | 1.954 | 1.921 | 1.969 | 1.933 | 1.904 | 1.924 | 1.869 | 1.906 |
| TOTAL | 2.000 | 2.000 | 2.000 | 2.000 | 2.000 | 2.000 | 2.000 | 2.000 |
| *Field #* | *B3A* | *B9* | *B3A* | *B7B* | *B7A* | *B3A* | *B2B* | *B20A* |

**Analysis of coexisting dolomite given in Table 3. Assemblages (minerals listed in order of decreasing abundance; those in trace amounts are in parentheses): 1. rieb-cal-dol-(mag); 2. dol-cal-stilp-(py); 3. stilp-qtz-cal-mag-(dol)-(rieb); 4. dol-rieb-cal-qtz-(stilp)-(mag); 5. mag-qtz-stilp-cal-dol; 6. qtz-mag-stilp-dol; 7. cal-rieb-(stilp)-(mag); 8. cal-rieb-dol-mag.*

representative electron probe analyses in Table 3. The complete range of these carbonates is shown in Figures 3a and b. The tieline distribution between dolomite (or ankerite)–siderite pairs shows considerable consistency although there are some tielines that cross the general trend.

Siderite was found only in the lower part of the Marra Mamba Formation. Representative electron probe analyses are given in Table 4, and the complete compositional range, which extends from $Fe_{50}Mg_{50}$ to just short of the Fe end-member composition, is shown in Figure 3b. The most Fe-rich siderites are also the most Ca-rich (up to 2.43% CaO).

Similar calcite–ankerite, and ankerite–siderite pairs are common in the Sokoman Iron Formation in Labrador, Canada (Klein and Fink, 1976), the Biwabik Iron Formation, Minnesota (French, 1968), and the Gunflint Iron Formation, Ontario, Canada (Floran and Papike, 1975). Haase (1979) reports a few calcite–ankerite and ankerite–siderite pairs from the least metamorphosed part of the Negaunee Iron Formation in northern Michigan. The compositional range of the carbonates from the above referenced occurrences is more restricted to the Fe-rich side of the diagrams in Figure 3, than is that of the carbonates in the Marra Mamba Iron Formation; many of the carbonates in this study are more magnesian than in other iron-formations.

### *Stilpnomelane*

Stilpnomelane is the most common Fe-silicate in the magnetite-rich, upper part of the Marra Mamba Iron Formation (B samples) as well as in the sulfide-rich, magnetite-free, lower part of the formation (A samples). Where stilpnomelane is present as a major constituent the rock is dark brown. Where present as layers between carbonate- or magnetite- or sulfide-

Table 3. Representative electron probe analyses of members of the dolomite–ankerite series. Analysis no. 1 is for a sample from the Wittenoon Dolomite but the other samples are all from the Marra Mamba Iron Formation.

| | 1 | 2 | 3 | 4 | 5* | 6** | 7* | 8** | 9** | 10 | 11 | 12 | 13 | 14 |
|---|---|---|---|---|---|---|---|---|---|---|---|---|---|---|
| FeO | 2.36 | 10.61 | 11.77 | 12.46 | 12.97 | 15.93 | 16.82 | 16.85 | 16.88 | 18.21 | 18.77 | 20.31 | 21.15 | 23.11 |
| MnO | 0.98 | 0.30 | 0.52 | 0.19 | 0.92 | 0.46 | 0.98 | 0.42 | 0.45 | 0.25 | 0.78 | 0.82 | 0.02 | 0.18 |
| MgO | 21.08 | 14.82 | 13.91 | 12.14 | 10.44 | 11.15 | 9.30 | 11.18 | 10.19 | 10.19 | 7.46 | 7.74 | 7.57 | 6.34 |
| CaO | 28.97 | 27.90 | 27.27 | 27.31 | 26.12 | 26.06 | 26.43 | 26.73 | 27.45 | 26.41 | 26.73 | 26.47 | 25.92 | 25.85 |
| Total | 53.39 | 53.63 | 53.47 | 52.10 | 50.45 | 53.60 | 53.53 | 55.18 | 54.97 | 55.06 | 53.74 | 55.34 | 54.66 | 55.48 |
| | recalculated on the basis of 2(Fe,Mn,Mg,Ca) | | | | | | | | | | | | | |
| Fe | 0.060 | 0.290 | 0.327 | 0.360 | 0.393 | 0.457 | 0.493 | 0.472 | 0.478 | 0.517 | 0.560 | 0.590 | 0.623 | 0.683 |
| Mn | 0.025 | 0.008 | 0.015 | 0.005 | 0.028 | 0.013 | 0.029 | 0.012 | 0.013 | 0.007 | 0.023 | 0.024 | 0.001 | 0.005 |
| Mg | 0.964 | 0.723 | 0.688 | 0.625 | 0.564 | 0.571 | 0.486 | 0.558 | 0.514 | 0.516 | 0.396 | 0.401 | 0.397 | 0.334 |
| Ca | 0.951 | 0.979 | 0.970 | 1.010 | 1.015 | 0.959 | 0.992 | 0.958 | 0.995 | 0.960 | 1.021 | 0.985 | 0.979 | 0.978 |
| Total | 2.000 | 2.000 | 2.000 | 2.000 | 2.000 | 2.000 | 2.000 | 2.000 | 2.000 | 2.000 | 2.000 | 2.000 | 2.000 | 2.000 |
| *Field #* | *B1* | *A26* | *A23B* | *A8* | *B3A* | *A58A* | *B7B* | *A10B* | *A24* | *A10B* | *B5A* | *B6B* | *A2A* | *A6A* |

**Analysis of coexisting calcite given in Table 2. **Analysis of coexisting siderite given in Table 4. Assemblages (minerals listed in order of decreasing abundance; those in trace amounts are in parentheses): 1. Wittenoom Dolomite: dol-(qtz)-(py)-(carbon); 2. qtz-dol; 3. qtz-dol-py-(stilp); 4. dol-stilp-green-py-(po); 5. stilp-qtz-cal-mag-(dol)-(rieb); 6. dol-sid-stilp; 7. dol-rieb-cal-qtz-(stilp)-(mag); 8. qtz-sid-dol-(minn)-(stilp); 9. dol-sid-po-py-stilp; 10. qtz-sid-dol-(minn)-(stilp); 11. mag-ank-stilp-qtz; 12. qtz-ank-stilp-mag; 13. stilp-ank-py-(minn)-(cp); 14. minn-ank.*

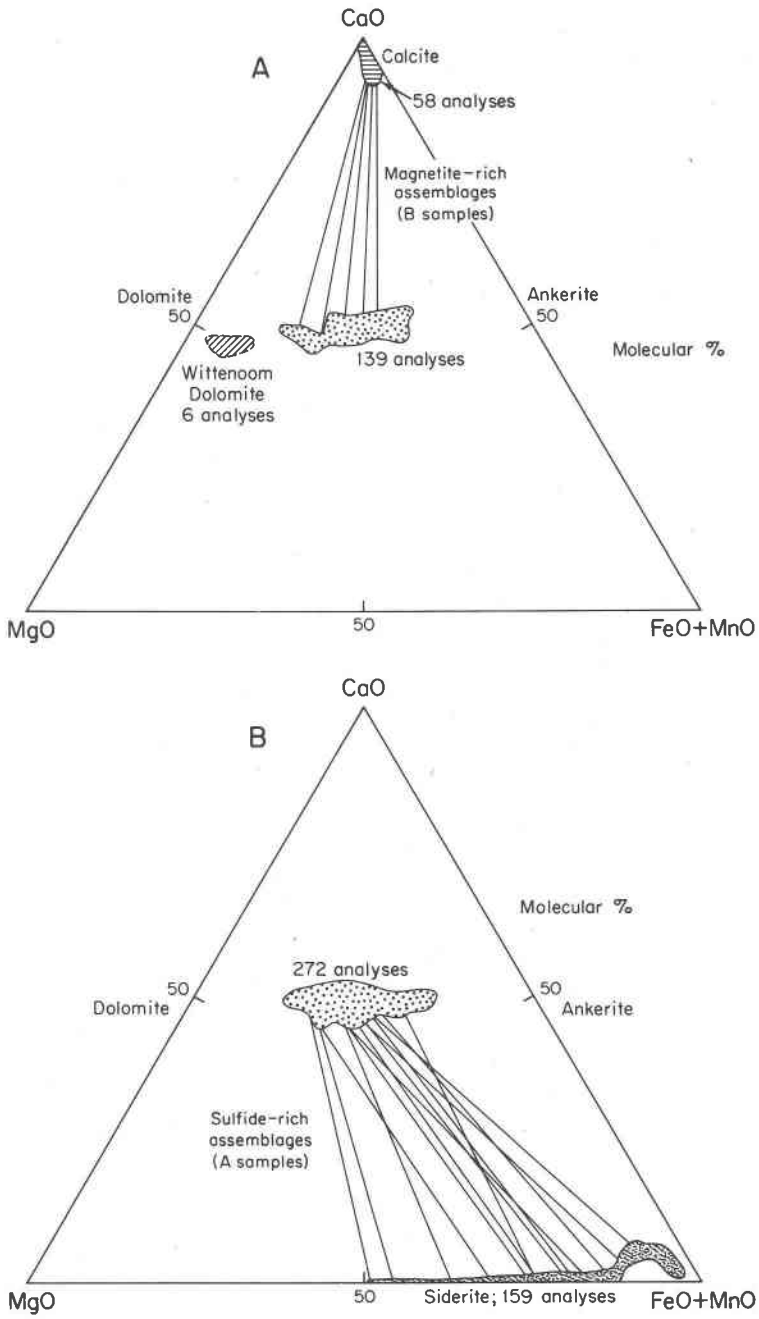


Fig. 3. Range of carbonate compositions and the chemistry of carbonate pairs (indicated by tielines) in (a) the upper, magnetite-rich part of the Marra Mamba Iron Formation and the Wittenoom Dolomite, and (b) the lower, sulfide-rich part of the Marra Mamba Iron Formation. The number of analyses comprising each compositional field is shown.

rich bands the rock appears well laminated. Stilpnomelane also occurs as well-crystallized sprays and globular aggregates.

Representative analyses of stilpnomelane are given in Table 5. The major chemical variation is in the Fe/(Fe+Mg) ratio, 0.587 to 0.825. $Al_2O_3$ contents range from 2.85 percent to 6.10 percent. The stilpnomelane compositions of the magnetite-rich part of the Marra Mamba Iron Formation (B samples) show a greater range in Fe/(Fe+Mg) ratios and a generally lower Al content than the stilpnomelanes in the magnetite-free, and sulfide-rich, lower part (A samples). These chemical relations are shown graphically in Figure 4. One of the assemblages (no. B10B) in the

magnetite-rich part of the Marra Mamba Iron Formation contains a 0.3 mm thick veinlet of a very fine-grained, light brown, matted, biotite-like material that cuts across a medium-grained assemblage of ferroan dolomite (Fe/(Fe+Mg) = 0.433) and stilpnomelane. Two representative analyses, given in Table 5 (nos. 9 and 10) show very high $K_2O$, $TiO_2$ and $Al_2O_3$ contents as compared with stilpnomelane (see also Fig. 4). Normal biotites tend to have somewhat higher $K_2O$ contents and considerably more $Al_2O_3$ than this phase which appears to be intermediate in composition between stilpnomelane and biotite. The MgO content is very much larger than that of any of the stilpnomelane analyzed in this study.

*Riebeckite*

Riebeckite is commonly present in the magnetite-rich, upper part of the Marra Mamba Iron Formation, but not as a major constituent of the samples studied. Old crocidolite workings within the Marra Mamba Formation indicate, however, that it is locally abundant (Trendall and Blockley, 1970). It is most commonly present as randomly distributed aggregates and sprays, although in places grains and patches may be aligned to form a poorly defined lamination. Table 6 lists representative analyses which have been recalculated by the method of Papike *et al.* (1974) to evaluate the $Fe^{3+}$ content. Although there is some range of Fe/(Fe+Mg) contents in the analyses, the general compositional range is remarkably small, as shown in Figure 5.

*Minnesotaite and Talc*

Sprays of minnesotaite are present in many of the assemblages, typically cutting quartz-carbonate- and stilpnomelane-rich assemblages. Table 7 gives representative electron microprobe analyses of minnesotaite and talc. The minnesotaite analyses show a large range of Fe/(Fe+Mg) ratios, 0.632 to 0.842. This range is similar to that of minnesotaite in the Sokoman Iron Formation (Klein, 1974) which ranges from about 0.64 to 0.92 (Fe+Mn)/(Fe+Mn+Mg) (Lesher, 1978). Two assemblages contain talc with an Fe/(Fe+Mg) ratio of 0.392 (analysis no. 7, able 7). The talc has a somewhat more coarsely bladed habit than is generally seen in the needlelike minnesotaite. Talc in iron-formation assemblages has also been reported by Floran and Papike (1975) from the Gunflint Iron Formation, by Lesher (1978) from the Sokoman Iron Formation , and by Gole and Klein (1981) from Archean iron-formations in Western Australia.

*Greenalite and Chlorite*

Greenalite is a very rare constituent of the Marra Mamba Iron Formation and is present in only two

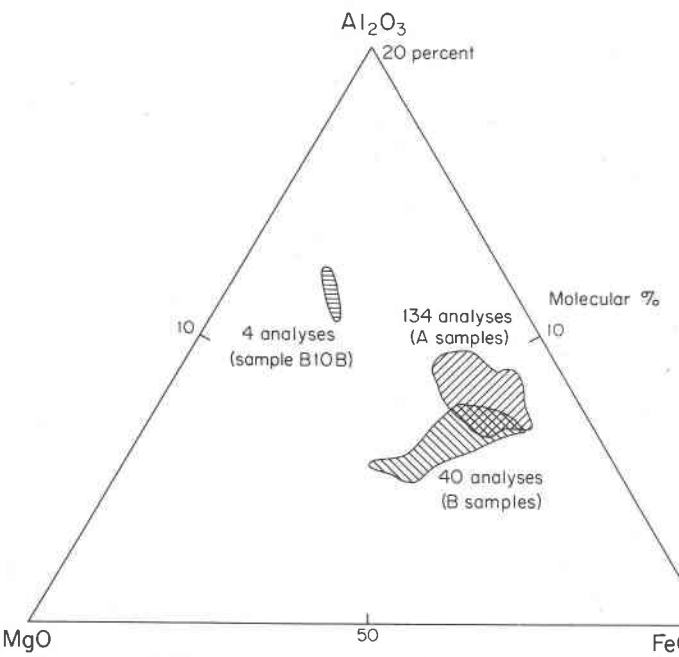


Fig. 4. Range of stilpnomelane compositions and that of a biotite-like phase in the Marra Mamba Iron-Formation, in terms of molecular percentages of MgO, FeO + MnO, and $Al_2O_3$. Note that the $Al_2O_3$ corner represents 20 molecular percent. The number of analyses comprising each compositional field is shown.

Table 4. Representative electron probe analyses of siderite in the Marra Mamba Iron Formation.

| | 1 | 2* | 3 | 4 | 5 | 6* | 7 | 8* | 9 | 10 | 11 |
|---|---|---|---|---|---|---|---|---|---|---|---|
| FeO | 36.09 | 43.87 | 44.02 | 47.00 | 50.14 | 49.96 | 51.98 | 50.16 | 53.07 | 54.55 | 56.06 |
| MnO | 1.41 | 0.90 | 0.84 | 0.35 | 0.27 | 0.21 | 0.05 | 0.84 | 0.07 | 0.05 | 0.00 |
| MgO | 19.68 | 12.08 | 10.06 | 9.50 | 9.45 | 7.04 | 5.35 | 2.27 | 0.78 | 0.90 | 1.08 |
| CaO | 0.16 | 0.16 | 0.17 | 0.53 | 0.30 | 0.48 | 0.19 | 2.71 | 2.43 | 1.87 | 1.03 |
| Total | 57.34 | 57.01 | 55.09 | 57.38 | 60.16 | 57.69 | 57.57 | 55.98 | 56.35 | 57.37 | 58.17 |
| | | | | | recalculated on the basis of 2(Fe,Mn,Mg,Ca) | | | | | | |
| Fe | 0.992 | 1.011 | 1.397 | 1.447 | 1.482 | 1.578 | 1.682 | 1.714 | 1.842 | 1.861 | 1.891 |
| Mn | 0.039 | 0.021 | 0.027 | 0.011 | 0.008 | 0.007 | 0.002 | 0.029 | 0.002 | 0.002 | 0.000 |
| Mg | 0.963 | 0.496 | 0.569 | 0.521 | 0.498 | 0.396 | 0.308 | 0.138 | 0.048 | 0.055 | 0.065 |
| Ca | 0.006 | 0.472 | 0.007 | 0.021 | 0.012 | 0.019 | 0.008 | 0.119 | 0.108 | 0.082 | 0.044 |
| Total | 2.000 | 2.000 | 2.000 | 2.000 | 2.000 | 2.000 | 2.000 | 2.000 | 2.000 | 2.000 | 2.000 |
| *Field #* | *A58A* | *A58A* | *A43B* | *A31* | *A13* | *A10B* | *A1* | *A24* | *A7A* | *A7B* | *A11B* |

**Analysis of coexisting dolomite or ankerite given in Table 3. Assemblages (minerals listed in order of decreasing abundance; those in trace amounts are in parentheses): 1. qtz-dol-sid-po-(carbon); 2. dol-sid-stilp; 3. qtz-sid-dol; 4. qtz-sid-minn; 5. sid-ank-stilp-qtz-(minn); 6. qtz-sid-dol-(minn)-(stilp); 7. stilp-sid-minn-py; 8. dol-sid-po-py-stilp; 9. sid-stilp-minn; 10. stilp-sid-py-minn; 11. sid-stilp-py.*

assemblages (A8 and B11B). In the A sample it occurs as light green, somewhat bladed (chlorite-like) patches that are closely intergrown with medium-grained stilpnomelane. The grain size of this greenalite is somewhat coarser than that of the typically cryptocrystalline variety that appears almost anisotropic in doubly polarized light (*e.g.*, Klein, 1974; Zajac, 1974; and Floran and Papike, 1975; Gole, 1980). In the B sample it occurs as medium-grained, light brownish green blotchy masses that are closely intergrown with irregular patches of pyrite and pyrrhotite. Feathery minnesotaite has grown at the expense of some of the greenalite. The habit of this greenalite is again not that of the usual cryptocrystalline variety, but as shown by the analyses in Table 8, it is compositionally very similar to greenalite analyzed by Floran and Papike (1975), Klein (1974) and Gole (1980).

Chlorite was found in only two samples (A37 and A37A) in which it occurs as very dense and fine-grained intergrowths with finely dispersed stilpnomelane. An analysis of this relatively Mg-rich phase is given in Table 8 (analysis no. 4).

### Assemblages and textures

The assemblages from the upper part of the Marra Mamba Iron Formation (B samples) are distinctly different from those of the lower section (A samples) (see Table 9). The majority of the B assemblages contain major amounts of quartz[2] and magnetite, and lesser and variable amounts of minnesotaite, riebeckite, stilpnomelane, dolomite (or ankerite), calcite, and traces of pyrite. The A samples, on the other hand, contain no iron oxides and no calcite. They consist of variable amounts of quartz, siderite, dolomite (or ankerite), stilpnomelane, minnesotaite, pyrrhotite and pyrite, and small amounts of carbon. The listing of coexistences in Table 9 illustrates the diversity of minerals that are intimately associated in the two complex types of iron-formation. The B samples would normally be classified as oxide-rich and the A samples as sulfide-rich (or type) iron-formation. Both types, however, contain abundant carbonates and silicates. The diversity of assemblages is caused mainly by fine scale banding and laminations in which alternating bands tend to have distinctly different mineralogies. Representative assemblages of both parts of the Marra Mamba Iron Formation are depicted in Figs. 6 and 7. The most common assemblages in the upper part (B samples) are: qtz-mag-dol-stilp-rieb-cal and qtz-mag-ank-stilp-rieb-minn (see Figs. 6a and

[2] Most of what is referred to as quartz has a grain size of <50 microns. As such it is a microcrystalline, finely granular quartz very similar to what is often referred to as chert.

Table 5. Representative electron probe analyses of stilpnomelane and a biotite-like phase in the Marra Mamba Iron Formation (columns 9 and 10).

| | 1 | 2 | 3 | 4 | 5 | 6 | 7 | 8 | 9 | 10 |
|---|---|---|---|---|---|---|---|---|---|---|
| $SiO_2$ | 47.44 | 47.83 | 48.04 | 48.67 | 48.82 | 45.68 | 48.15 | 51.33 | 42.62 | 43.40 |
| $TiO_2$ | 0.00 | 0.00 | 0.07 | 0.01 | 0.00 | 0.00 | 0.00 | 0.00 | 0.92 | 0.81 |
| $Al_2O_3$ | 4.81 | 3.99 | 4.03 | 3.99 | 4.69 | 6.10 | 5.40 | 2.85 | 8.78 | 9.13 |
| FeO | 33.46 | 33.08 | 30.76 | 30.91 | 29.51 | 29.26 | 27.59 | 29.64 | 16.31 | 15.08 |
| MnO | 0.06 | 0.15 | 0.05 | 0.05 | 0.06 | 0.08 | 0.07 | 0.06 | 0.01 | 0.19 |
| MgO | 3.98 | 4.08 | 5.73 | 5.84 | 7.09 | 7.46 | 7.55 | 10.54 | 17.27 | 17.43 |
| CaO | 0.02 | 0.04 | 0.10 | 0.10 | 0.18 | 0.02 | 0.29 | 0.07 | 0.10 | 0.02 |
| $Na_2O$ | 0.34 | 0.11 | 0.11 | 1.13 | 0.22 | 0.78 | 0.16 | 0.30 | 0.17 | 0.00 |
| $K_2O$ | 1.44 | 0.95 | 1.04 | 1.93 | 1.50 | 1.03 | 2.99 | 0.73 | 6.58 | 6.78 |
| Total | 91.55 | 90.23 | 89.93 | 92.63 | 92.07 | 90.41 | 92.20 | 92.52 | 92.76 | 92.84 |
| | recalculated on the basis of 11 oxygens (total Fe as $Fe^{2+}$ only) | | | | | | | | | |
| Si | 3.764 | 3.830 | 3.815 | 3.784 | 3.765 | 3.608 | 3.714 | 3.851 | 3.210 | 3.241 |
| Al | 0.236 | 0.170 | 0.185 | 0.216 | 0.235 | 0.392 | 0.286 | 0.149 | 0.779 | 0.759 |
| Σ | 4.000 | 4.000 | 4.000 | 4.000 | 4.000 | 4.000 | 4.000 | 4.000 | 3.989 | 4.000 |
| Al | 0.214 | 0.207 | 0.192 | 0.150 | 0.192 | 0.176 | 0.204 | 0.103 | 0.000 | 0.045 |
| Ti | 0.000 | 0.000 | 0.004 | 0.001 | 0.000 | 0.000 | 0.000 | 0.000 | 0.052 | 0.045 |
| Fe | 2.220 | 2.215 | 2.043 | 2.010 | 1.904 | 1.933 | 1.780 | 1.672 | 1.028 | 0.942 |
| Mn | 0.004 | 0.010 | 0.004 | 0.003 | 0.004 | 0.005 | 0.005 | 0.004 | 0.000 | 0.012 |
| Mg | 0.471 | 0.487 | 0.678 | 0.677 | 0.815 | 0.878 | 0.868 | 1.178 | 1.939 | 1.940 |
| Ca | 0.001 | 0.003 | 0.008 | 0.008 | 0.015 | 0.002 | 0.024 | 0.005 | 0.008 | 0.001 |
| Na | 0.052 | 0.017 | 0.017 | 0.170 | 0.033 | 0.120 | 0.024 | 0.044 | 0.025 | 0.000 |
| K | 0.146 | 0.097 | 0.105 | 0.191 | 0.148 | 0.104 | 0.295 | 0.070 | 0.632 | 0.646 |
| Σ | 3.108 | 3.036 | 3.051 | 3.210 | 3.111 | 3.218 | 3.200 | 3.076 | 3.684 | 3.631 |
| $\frac{Fe}{(Fe+Mg)}$ | 0.825 | 0.820 | 0.751 | 0.748 | 0.700 | 0.688 | 0.672 | 0.587 | 0.346 | 0.327 |
| *Field #* | *A8* | *B13B* | *B11B* | *A11B* | *A35B* | *A58A* | *A38* | *B12A* | *B10B* | *B10B* |

*Assemblages (minerals listed in order of decreasing abundance; those in trace amounts are in parentheses): 1. dol-stilp-green-py-(po); 2. ank-stilp-mag-minn-qtz; 3. qtz-mag-ank-stilp-minn; 4. sid-stilp-py-minn-(cp); 5. stilp-ank-po-(minn)-(qtz); 6. dol-sid-stilp; 7. dol-qtz-stilp; 8. dol-rieb-mag-stilp-qtz-py; 9 and 10. dol-stilp-(mag) traversed by veinlet of biotite-like material.*

Table 6. Representative electron probe analyses of riebeckite in the magnetite-rich part of the Marra Mamba Iron Formation (B samples only).

| | 1 | 2 | 3 | 4 | 5 | 6 |
|---|---|---|---|---|---|---|
| $SiO_2$ | 52.11 | 51.65 | 53.60 | 52.88 | 52.47 | 52.90 |
| $TiO_2$ | 0.38 | 0.00 | 0.13 | 0.00 | 0.07 | 0.16 |
| $Al_2O_3$ | 0.07 | 0.08 | 0.19 | 0.01 | 0.14 | 0.04 |
| FeO | 31.02 | 30.96 | 30.41 | 29.44 | 29.38 | 26.29 |
| MnO | 0.03 | 0.02 | 0.15 | 0.00 | 0.07 | 0.01 |
| MgO | 4.38 | 4.85 | 5.38 | 6.08 | 6.98 | 7.71 |
| CaO | 0.46 | 0.41 | 0.75 | 0.59 | 0.33 | 0.29 |
| $Na_2O$ | 7.15 | 7.68 | 6.48 | 6.26 | 6.31 | 7.30 |
| $K_2O$ | 0.03 | 0.00 | 0.01 | 0.15 | 0.08 | 0.04 |
| Total | 95.63 | 95.65 | 97.10 | 95.41 | 95.83 | 94.74 |
| $Fe_2O_3$* | 13.51 | 11.08 | 15.89 | 15.58 | 11.28 | 13.68 |
| FeO | 18.86 | 20.99 | 16.11 | 15.40 | 19.23 | 13.98 |
| Total | 96.98 | 96.76 | 98.69 | 96.95 | 96.96 | 96.11 |
| recalculated on the basis of 23 oxygens | | | | | | |
| Si | 7.993 | 7.992 | 7.986 | 7.999 | 7.987 | 7.996 |
| Al | 0.007 | 0.008 | 0.014 | 0.001 | 0.013 | 0.004 |
| Σ | 8.000 | 8.000 | 8.000 | 8.000 | 8.000 | 8.000 |
| Al | 0.006 | 0.007 | 0.019 | 0.001 | 0.012 | 0.003 |
| Ti | 0.044 | 0.000 | 0.015 | 0.000 | 0.008 | 0.018 |
| $Fe^{3+}$ | 1.560 | 1.290 | 1.781 | 1.753 | 1.292 | 1.557 |
| $Fe^{2+}$ | 2.420 | 2.716 | 2.008 | 1.972 | 2.448 | 1.767 |
| Mn | 0.004 | 0.003 | 0.019 | 0.000 | 0.009 | 0.001 |
| Mg | 1.001 | 1.119 | 1.194 | 1.370 | 1.584 | 1.737 |
| Σ | 5.035 | 5.135 | 5.036 | 5.096 | 5.353 | 5.083 |
| XOCT | 0.035 | 0.135 | 0.036 | 0.096 | 0.353 | 0.083 |
| Ca | 0.075 | 0.068 | 0.120 | 0.096 | 0.054 | 0.047 |
| Na | 1.890 | 1.797 | 1.844 | 1.808 | 1.593 | 1.870 |
| | 2.000 | 2.000 | 2.000 | 2.000 | 2.000 | 2.000 |
| Na | 0.237 | 0.507 | 0.028 | 0.027 | 0.269 | 0.270 |
| K | 0.006 | 0.000 | 0.002 | 0.029 | 0.016 | 0.008 |
| | 0.243 | 0.507 | 0.030 | 0.056 | 0.285 | 0.278 |
| Total | 15.278 | 15.507 | 15.030 | 15.056 | 15.285 | 15.278 |
| $\frac{Fe\ total}{(Fe+Mg)}$ | 0.799 | 0.782 | 0.760 | 0.731 | 0.702 | 0.657 |
| *Field #* | *B14C* | *B4C* | *B13A* | *B12A* | *B2B* | *B4C* |

*$Fe_2O_3$ content estimated by the method of Papike et. al. (1974).

*Assemblages (minerals are listed in order of decreasing abundance; those in trace amounts are in parentheses): 1. cal-rieb-(stilp)-(py); 2. qtz-rieb-dol-cal-mag; 3. cal-dol-qtz-(rieb)-(py); 4. dol-rieb-mag-stilp-qtz-py; 5. cal-rieb-(stilp)-(mag); 6. qtz-rieb-dol-cal-mag.*

b). The most common types in the lower section of the Marra Mamba (A samples) are: qtz-dol(or ank)-stilp-sid-py-po and qtz-dol(or ank)-sid-stilp-minn-po-py (see Figs. 7a and b). The assemblages shown in Figs. 6 and 7, and listed in Table 9 may not all be equilibrium assemblages. It has been impossible for us, at the very low temperatures these assemblages have undergone, to differentiate equilibrium and disequilibrium coexistences.

The grain sizes of the assemblages are mainly fine to very fine. Quartz is often microcrystalline and chert-like in handspecimen as well as in grain size in transmitted light. The carbonates are generally considerably coarser grained than quartz (or chert) and tend to have euhedral, rhombohedral outlines (see Figs. 8c to e). Magnetite shows a range of grain sizes from fine- to medium-grained, and generally good octahedral outline unless the grains are severely crowded together in essentially continuous microbands or laminations (see Figs. 9b to c). Stilpnomelane occurs as discontinuous laminations of finely matted intergrowths of thin sheaves (see Fig. 9a), and also as coarser grained sprays and rosettes of subhedral sheaves (Figs. 8a and c). Minnesotaite displays its typical habit of randomly distributed rosettes of needles in carbonate and quartz (or chert) matrices. Its cross-cutting relations with stilpnomelane and carbonates are clear evidence for it having formed subsequent to the minerals it transgresses. A coarser grained variety is found in close association with pyrite grains (Fig. 8b). Riebeckite ranges from fine- to medium-grain size and occurs as randomly distributed grains in qtz-dol(or ank)-stilp-mag matrices, or as thin laminations that parallel quartz-magnetite microbands. Frequently the riebeckite needles are very fine and elongate (see Fig. 8e) and cut across

Table 7. Representative electron probe analyses of minnesotaite and talc.

| | 1 | 2 | 3 | 4 | 5 | 6 | 7 |
|---|---|---|---|---|---|---|---|
| $SiO_2$ | 48.87 | 49.20 | 50.65 | 51.36 | 52.13 | 51.61 | 54.40 |
| $TiO_2$ | 0.00 | 0.00 | 0.00 | 0.02 | 0.00 | 0.05 | 0.00 |
| $Al_2O_3$ | 1.15 | 0.67 | 0.49 | 0.57 | 0.56 | 0.84 | 1.09 |
| FeO | 37.59 | 36.36 | 33.11 | 32.13 | 30.91 | 29.59 | 20.20 |
| MnO | 0.01 | 0.00 | 0.04 | 0.19 | 0.07 | 0.24 | 0.08 |
| MgO | 3.94 | 4.57 | 7.00 | 7.80 | 8.18 | 9.65 | 17.55 |
| CaO | 0.00 | 0.01 | 0.00 | 0.00 | 0.00 | 0.01 | 0.00 |
| $Na_2O$ | 0.00 | 0.02 | 0.19 | 0.00 | 0.00 | 0.03 | 0.00 |
| $K_2O$ | 0.42 | 0.22 | 0.32 | 0.44 | 0.47 | 0.62 | 0.12 |
| Total | 90.98 | 91.05 | 91.80 | 92.51 | 92.32 | 92.64 | 93.44 |
| recalculated on the basis of 11 oxygens (Fe total as $Fe^{2+}$ only) | | | | | | | |
| Si | 3.889 | 3.951 | 3.959 | 3.959 | 3.991 | 3.927 | 3.887 |
| Al | 0.110 | 0.049 | 0.041 | 0.041 | 0.009 | 0.073 | 0.092 |
| Σ | 3.999 | 4.000 | 4.000 | 4.000 | 4.000 | 4.000 | 3.979 |
| Al | 0.000 | 0.014 | 0.005 | 0.011 | 0.042 | 0.002 | 0.000 |
| Ti | 0.000 | 0.000 | 0.000 | 0.001 | 0.000 | 0.003 | 0.000 |
| Fe | 2.554 | 2.441 | 2.164 | 2.071 | 1.979 | 1.883 | 1.207 |
| Mn | 0.001 | 0.000 | 0.002 | 0.013 | 0.005 | 0.015 | 0.004 |
| Mg | 0.478 | 0.547 | 0.816 | 0.896 | 0.934 | 1.094 | 1.869 |
| Ca | 0.000 | 0.000 | 0.000 | 0.000 | 0.000 | 0.001 | 0.000 |
| Na | 0.000 | 0.003 | 0.028 | 0.000 | 0.000 | 0.004 | 0.000 |
| K | 0.044 | 0.023 | 0.032 | 0.044 | 0.046 | 0.061 | 0.011 |
| Σ | 3.077 | 3.028 | 3.047 | 3.036 | 3.006 | 3.063 | 3.091 |
| $\frac{Fe}{(Fe+Mg)}$ | 0.842 | 0.817 | 0.726 | 0.698 | 0.679 | 0.632 | 0.392 |
| *Field #* | *A7B* | *A6A* | *A28A* | *B11B* | *B13B* | *B5B* | *B2B* |

*Assemblages (minerals listed in order of decreasing abundance; those in trace amounts are in parentheses): 1. stilp-sid-py-minn; 2. minn-ank; 3. qtz-minn-stilp-ank-po; 4. qtz-minn-green-po-py; 5. ank-minn-qtz-mag; 6. qtz-mag-minn; 7. dol-qtz-stilp-tc-(mag).*

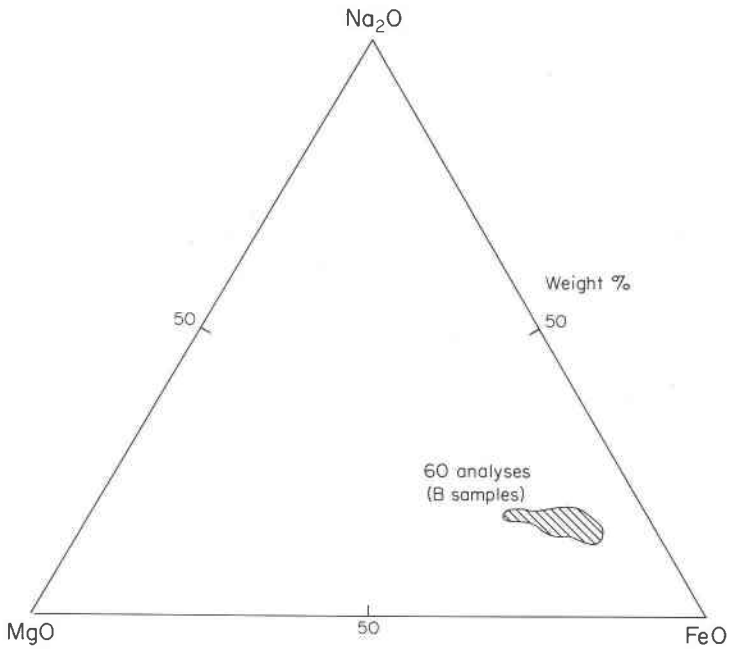


Fig. 5. Range of riebeckite compositions in the magnetite-rich, upper part of the Marra Mamba Iron Formation, in terms of weight percentage of $Na_2O$, MgO, and FeO (total Fe and FeO). The number of analyses comprising the compositional field is shown.

other minerals, such as quartz and carbonates. Pyrite and pyrrhotite are common constituents of the sulfide type iron-formation. Pyrite is commonly medium-grained and euhedral, whereas pyrrhotite is anhedral, mostly granular in habit (see Fig. 8f). Both sulfides may occur together and generally define thin (< 1 mm thick) discontinuous bands, parallel to the banding of other surrounding rock types.

Fine-scale banding and laminations are common within mesobands (see Figs. 9a and b) but microbanding as described by Trendall and Blockley (1970) and Trendall (1973) in the Dales Gorge Member and the Weeli Wolli Formation of the Hamersley Group, is in general poorly developed (see also Ewers and Morris, 1980). The continuity of fine laminations is commonly interrupted by well-crystallized, medium-grained rhombohedral carbonates, as well as recrystallized magnetite of medium grain size (see Fig. 9c). Although pyrite and pyrrhotite, in the sulfide-rich iron-formation, are most commonly present as finely disseminated grains, they also occur as well-defined bands (up to several mm in thickness) and laminations of dense concentrations of subhedral pyrrhotite and/or pyrite grains (see Fig. 9d).

## Discussion and conclusions

The magnetite-containing assemblages of the Marra Mamba Iron Formation are very similar to those reported for the weakly metamorphosed parts of the Sokoman (Klein, 1974 and 1978; Klein and Fink, 1976; Zajac, 1974; Lesher, 1978), the Negaunee (James, 1955; Haase, 1979), the Biwabik (French, 1968) and Gunflint Iron Formations (Floran and Papike, 1975) except for the abundant presence of riebeckite and the general absence of greenalite. The averaged bulk composition for the nine samples of the Marra Mamba Iron Formation versus those of the Sokoman or Biwabik Iron Formations (Gole and Klein, 1981) reveals a considerably higher $Na_2O$ content (0.39%) than for the other two (Sokoman 0.17 and Biwabik 0.06%). The average for the four magnetite-rich samples in Table 1 gives a value of 0.43 wt.% $Na_2O$.

The medium- to coarse-grained, sub- to euhedral outlines of the carbonates and magnetite are very similar in all of the iron-formations mentioned above. Medium- to coarse-grained stilpnomelane patches and sprays appear to be universal, and minnesotaite shows cross-cutting relations with carbonates and stilpnomelane (as well as greenalite when present) in many occurrences. Riebeckite grains are common as part of the fine- to medium-grained matrix of the Marra Mamba Iron Formation or as small rosettes and sprays of delicate and long needles, but very rare in most of the North American occurrences. Such riebeckite, as is also the case for minnesotaite,

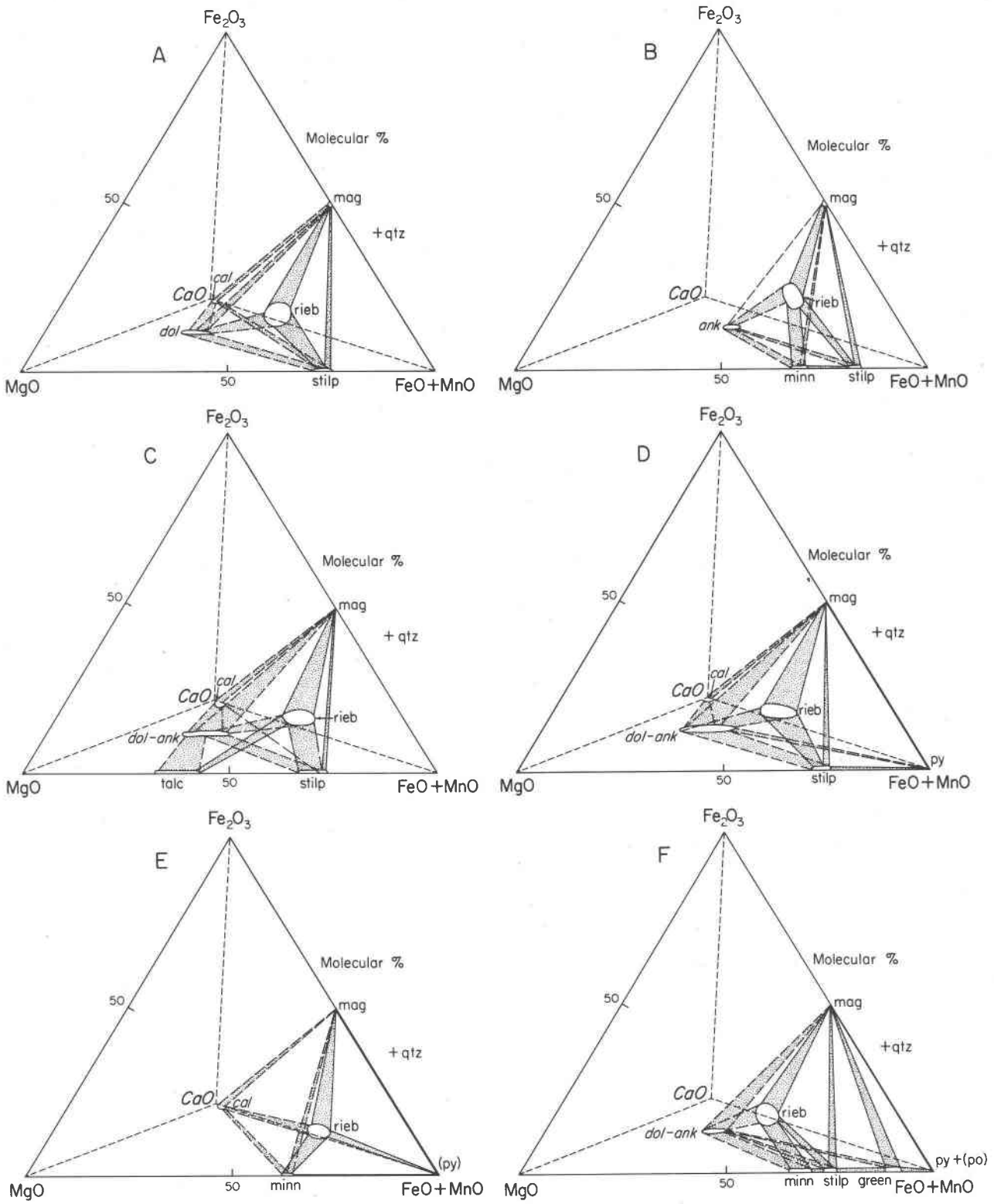


Fig. 6. Graphical representation of assemblages in the magnetite-rich part of the Marra Mamba Iron Formation (B samples) in terms of important and competing solid solution components, molecular percentages of CaO, MgO, (FeO+MnO), and $Fe_2O_3$. Mineral abbreviations as in Table 1. Coexistences shown in A and B are the most common.

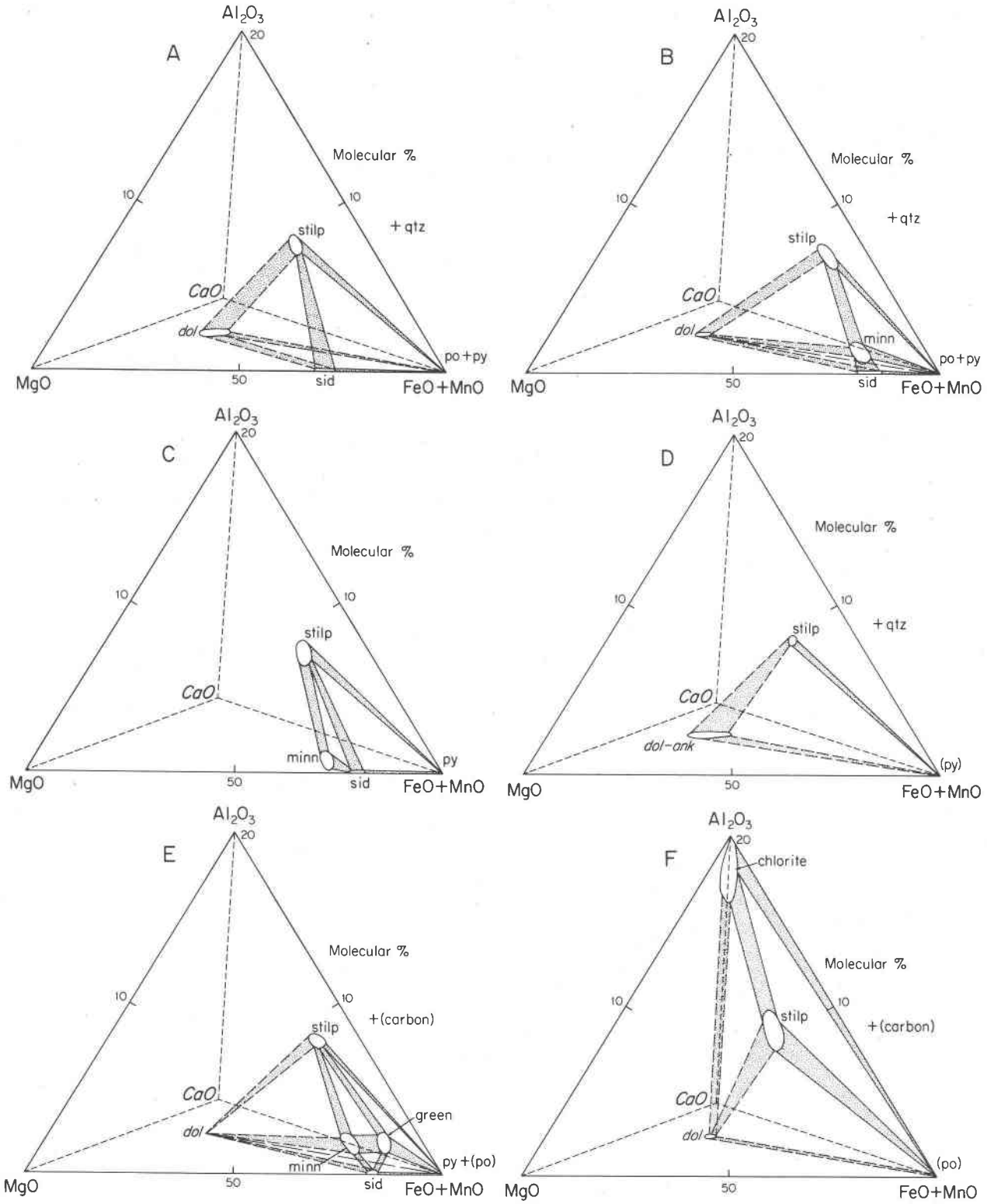


Fig. 7. Graphical representation of assemblages in the sulfide-rich part of the Marra Mamba Iron Formation (A samples) in terms of important and competing solid solution components, molecular percentages of CaO, MgO, (FeO+MnO), and $Al_2O_3$. The $Al_2O_3$ apex represents 20 mole%. Mineral abbreviations as in Table 1. Coexistences shown in A and B are the most common.

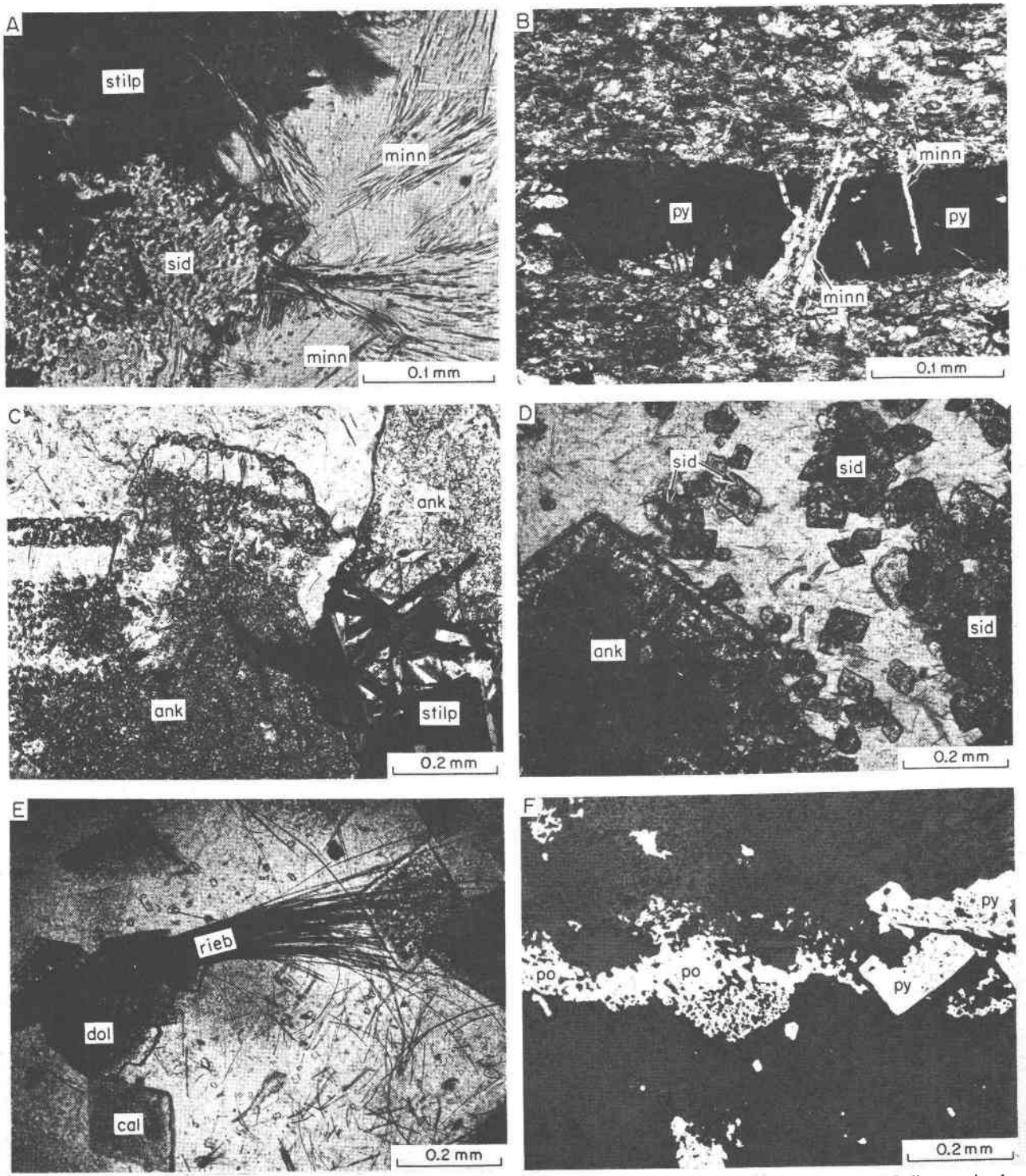


Fig. 8. Photomicrographs of representative assemblages and textures in the Marra Mamba Iron Formation. A. Medium-grained siderite and light brown, fine-grained stilpnomelane overprinted by minnesotaite. Plane polarized light (#A11B). B. Medium-grained pyrite (opaque) intergrown with minnesotaite, in a fine-grained matrix of stilpnomelane, ankerite and extremely fine minnesotaite needles. Minnesotaite is commonly medium- to coarse-grained when intergrown with pyrite. Plane polarized light (#A2A). C. Coarse-grained, anhedral ankerite grains intergrown with medium-grained, dark brown sheaves of stilpnomelane. The ankerite has abundant small quartz inclusions but a quartz-free rim. It is not compositionally zoned. Plane polarized light (#A18). D. Coarse euhedra of ankerite and smaller, euhedral grains of siderite in a fine-grained quartz-minnesotaite matrix. Plane polarized light (#A33). E. Extremely fine needles of riebeckite in a matrix of fine-grained quartz and well-crystallized euhedra of dolomite and calcite. Magnetite is also part of this assemblage but is not present in the photograph. Plane polarized light (#B4C). F. Discontinuous bands of euhedral, medium-grained pyrite and anhedral pyrrhotite in a matrix of fine-grained quartz and medium-grained dolomite (to ankerite). Reflected, plane polarized light (#A23B).

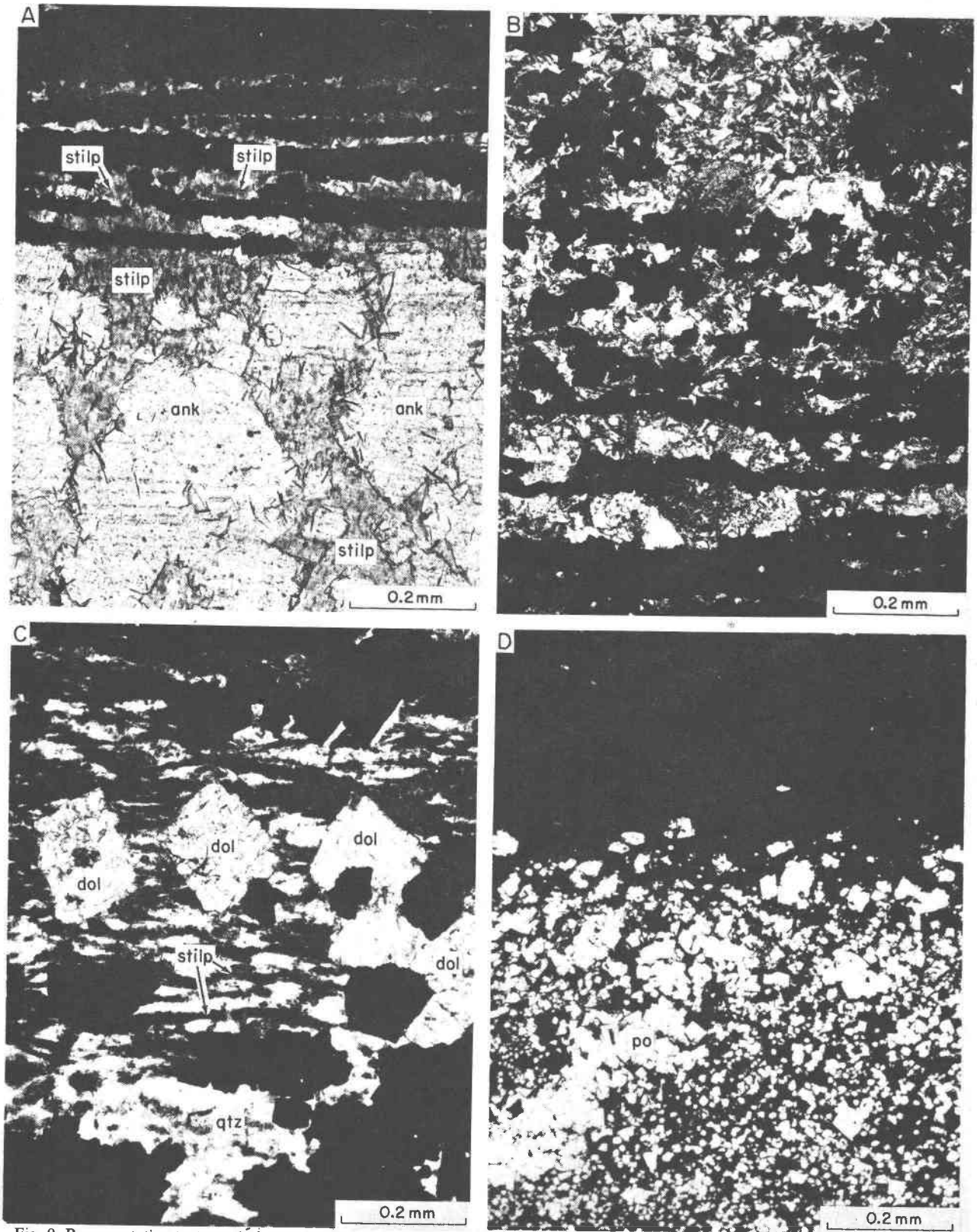


Fig. 9. Representative textures (primary structures) in the Marra Mamba Iron Formation. A. Medium-grained magnetite (opaque)-stilpnomelane mesoband adjoining an ankerite-stilpnomelane mesoband in which the ankerite is coarsely recrystallized. Plane polarized light (#B6B). B. Magnetite laminations (opaque) across a matrix of medium-grained dolomite, with minor stilpnomelane and quartz. Doubly polarized light (#B8A). C. Medium-grained dolomite and magnetite (opaque) euhedra in fine-grained, laminated matrix of stilpnomelane and quartz. Plane polarized light (#B2B). D. Fine- to medium-grained pyrrhotite-rich mesoband adjoining a fine-grained stilpnomelane-chlorite mesoband. Reflected, plane polarized light (#A37A).

Table 8. Representative electron probe analyses of greenalite (columns 1, 2 and 3) and chlorite (column 4).

| | 1 | 2 | 3 | 4 |
|---|---|---|---|---|
| $SiO_2$ | 36.13 | 34.96 | 36.26 | 29.17 |
| $TiO_2$ | 0.09 | 0.00 | 0.09 | 0.00 |
| $Al_2O_3$ | 0.03 | 1.37 | 1.07 | 15.57 |
| FeO | 50.02 | 49.23 | 47.98 | 28.20 |
| MnO | 0.19 | 0.00 | 0.02 | 0.00 |
| MgO | 2.49 | 3.04 | 3.44 | 13.30 |
| CaO | 0.03 | 0.05 | 0.01 | 0.44 |
| $Na_2O$ | 0.10 | 0.04 | 0.01 | 0.06 |
| $K_2O$ | 0.00 | 0.00 | 0.02 | 0.06 |
| Total | 89.08 | 88.69 | 88.90 | 86.80 |
| | on basis of 14 oxygens | | | |
| Si | 4.276 | 4.142 | 4.235 | 3.145 |
| Al | - | - | - | 0.855 |
| Al | 0.004 | 0.191 | 0.147 | 1.124 |
| Ti | 0.008 | 0.000 | 0.007 | 0.000 |
| Fe | 4.950 | 4.879 | 4.686 | 2.543 |
| Mn | 0.019 | 0.000 | 0.002 | 0.000 |
| Mg | 0.439 | 0.537 | 0.600 | 2.137 |
| Ca | 0.004 | 0.007 | 0.002 | 0.051 |
| Na | 0.022 | 0.009 | 0.002 | 0.013 |
| K | - | 0.000 | 0.003 | 0.008 |
| | 5.446 | 5.623 | 5.449 | 5.876 |
| $\frac{Fe}{(Fe+Mg)}$ | 0.918 | 0.901 | 0.886 | 0.543 |
| *Field #* | *B11B* | *A8* | *A8* | *A37A* |

*Assemblages (minerals are listed in order of decreasing abundance; those in trace amounts are in parentheses): 1. qtz-minn-green-py-po; 2 and 3. stilp-py-green-dol-(minn)-(po); 4. stilp-chl-(carbon)-(po)-(ilm).*

appears to have formed during the late diagenetic to very low-grade metamorphic stages of the iron-formation (Milton and Eugster 1959; Trendall and Blockley, 1970).

The sulfide-rich assemblages of the Marra Mamba Iron Formation are an example of the sulfide-type iron-formation, originally described as "sulfide-facies" by James (1954). These assemblages reflect considerably more reducing sedimentary conditions than the magnetite-rich associations (Klein and Bricker, 1977). This is reflected in the much lower $Fe^{3+}/(Fe^{2+}+Fe^{3+})$ ratios of the sulfide-rich part (0 to 0.18) *versus* those of the magnetite-rich part (0.49 to 0.55; see Table 1).

The primary structures of the Marra Mamba Iron Formation are very similar to those in other members of the Hamersley Group (Trendall and Blockley, 1970) and in Archean iron-formations described by Gole (1980). Fine-scale laminations and banding are the only sedimentary textures in the Marra Mamba whereas oolitic and granular textures are commonly present in North American sequences as well (Gole and Klein, 1981).

The question of the possible metamorphic history of the Marra Mamba Iron Formation is a difficult one. Quartz which is a major constituent is generally microcrystalline. Unambiguous overprints of minnesotaite and riebeckite on earlier minerals, such as carbonates and stilpnomelane, are abundant. Both of these minerals have large stability fields in terms of temperature and pressure. Talc, the Mg-rich phase which is closely related to minnesotaite, can be formed experimentally at 90°C and atmospheric pressure (Bricker *et al.*, 1973). Minnesotaite, therefore, will be stable over a wide range of pressure-temperature conditions, ranging from a minimum of that determined for talc to maximal conditions of those associated with the transition from the biotite to garnet zones, as shown by pelitic schists (Klein, 1978). Riebeckite ranges in stability from late diagenetic (Milton and Eugster, 1959) to that of high grades of metamorphism (Ernst, 1962). Other minerals of the iron-formation have similarly large, if not larger pressure-temperature stability fields (*e.g.*, carbonates, magnetite, stilpnomelane).

The presence and distribution of authigenic prehnite, pumpellyite, epidote and actinolite as very low grade metamorphic minerals in basic and intermediate volcanics of the Fortescue Group (which directly underlies the Hamersley Group) has been documented by Smith (1980) and Smith *et al.* (1981). These authors interpret four sub-greenschist to greenschist facies metamorphic zones. These are: ZI—pumpellyite + prehnite; ZII—pumpellyite + prehnite + epidote; ZIII—pumpellyite + prehnite + epidote + actinolite; and ZIV—epidote + actinolite + prehnite. The samples of the present study can be placed within those authors' zone II by reference to their reconstructed cross section. This would imply temperatures, during burial, in the range of 200° to 300°C and a maximum pressure of burial of about 1.2 kbar for the Marra Mamba Iron Formation. Oxygen isotope temperature estimates (Becker and Clayton, 1976) on the overlying Dales Gorge Member

Table 9. Complete listing of assemblages in the magnetite-rich (B samples) and sulfide-rich (A samples) portions of the Marra Mamba Iron Formation.

| B samples | | | | | | | | | | | |
|---|---|---|---|---|---|---|---|---|---|---|---|
| qtz | mag | stilp | minn | green | rieb | tc | cal | dol | ank | py | po |
| X | X | | | | | | | | | | |
| X | X | | X | | | | | | | | |
| X | X | | X | | | | X | X | | | |
| X | X | X | X | | | | | X | | | |
| X | X | X | X | | | | | | X | | |
| X | X | X | | | | | | X | | | |
| X | X | X | | | | X | | X | | | |
| X | X | X | | | | | | | X | | |
| X | X | X | | | | | X | X | | (X) | |
| X | X | X | | | | | X | | | | |
| X | X | | | | X | | | | | | |
| X | X | | | | X | | | X | | | |
| X | X | | (X) | | X | | X | X | | (X) | |
| X | X | X | | | X | | | X | | | |
| X | X | X | | | (X) | (X) | | | X | | |
| X | X | | | | (X) | | X | X | | (X) | |
| X | X | | | | X | | X | | | (X) | |
| X | X | | | | X | X | | | | | |
| X | | | | | X | | | X | | (X) | |
| X | | | | | X | | | | X | | |
| X | | X | | | | X | | X | | | |
| X | | | X | | | | | | X | | |
| X | | | X | X | | | | | | X | X |
| X | | | | | | | | | | | |
| X | | X | | | | | X | | X | | |
| | X | X | | | | | | X | | | |
| | X | X | | | X | | | X | | | |
| | X | | | | X | | X | X | | | |
| | X | X | | | X | | X | | | | |
| | | X | | | X | | X | | | (X) | |
| | | X | | | | | X | | | | |
| | | X | | | | | X | X | | (X) | |
| | | X | | | | | X | X | | (X) | |
| | | X | | | X | | | X | | (X) | |
| | X | | X | | | | | | X | | |
| | | | | | X | | | | X | (X) | |

| A samples | | | | | | | | | | | | |
|---|---|---|---|---|---|---|---|---|---|---|---|---|
| qtz | stilp | minn | green | chlor | dol | ank | sid | py | po | cp | ilm | carbon |
| X | | X | | | | | X | | | | | |
| X | | X | | | | | X | X | | | | |
| X | | X | | | | | X | | X | | | |
| X | X | X | | | | X | X | | | | | |
| X | X | | | | | | X | | X | | | |
| X | | X | | | | X | | X | X | | | |
| X | X | | | | | | X | X | X | (X) | | |
| X | X | X | | | | | X | | | | | (X) |
| X | X | | | | X | | | | | | | |
| X | X | | | | X | | | X | | | | |
| X | | | | | X | | X | | | | | |
| X | X | | | | X | | | X | X | | | |
| X | X | | | | X | | X | X | X | (X) | | |
| X | | X | | | X | X | | | X | | | |
| X | X | X | | | X | X | | | | | | |
| X | X | X | | | | | | | X | | | (X) |
| X | X | | | | | | | | | | | (X) |
| X | X | X | | | | | | | | | | |
| X | X | | | | | | | | | | | |
| X | X | | | | | | | | X | | | |
| X | X | | | | X | | | | X | | | |
| X | X | | | | | X | X | | X | | | |
| X | X | X | | | | | X | X | (X) | | | |
| X | X | X | | | | X | | (X) | (X) | | | |
| | X | | | | | | | | | | | |
| | X | X | | | | | X | | | (X) | | |
| | X | X | | | | X | | | | (X) | | |
| | X | X | | | | X | | | | | | |
| | X | | | | X | | | | | | | |
| | X | | | | X | | | X | | | | |
| | X | X | | | X | | | | | | | |
| | X | | X | | X | | | (X) | | | | |
| | X | | X | | X | | | X | (X) | | | |
| | X | | X | X | | | | X | (X) | | | |
| | X | | | | | | | (X) | | | | (X) |
| | X | | | X | X | | | | | | | |
| | X | | | X | | | | (X) | | | (X) | (X) |
| | X | | | X | | | | | X | (X) | | |
| | | X | | | | X | | | | | | |
| | X | X | | | | X | | | | | | |
| | | X | | | | | X | X | | | | |
| | X | | | | X | | | | (X) | | | (X) |
| | X | | | | X | | | | (X) | | | |
| | X | | | | X | | | (X) | X | | | |
| | X | | | | X | | X | | (X) | | (X) | |
| | X | | | | | X | | | X | | | |
| | X | | | | | | X | X | | | | |
| | X | | | | | | X | (X) | | | | (X) |

*Mineral abbreviations as in Table 1; X = major component; (X) = trace amount.*

*For relatively homogeneous mesobands the assemblage listing reflects the mineralogy of an area in a thin section of 5 to 10 mm in diameter; in finely banded or laminated rock types the assemblage listing may reflect the mineralogy of a band <0.3 mm in thickness.*

and Wittenoom Dolomite indicate temperatures of burial for those formations of 270 to 310°C. The almost total lack of greenalite in materials of this study might well be the result of such elevated temperatures. The low temperature metamorphic assemblages of iron-formation are, however, relatively insensitive to changes in metamorphic temperature on account of the large stability fields of their low temperature index minerals. Because of this, as well as a lack of knowledge of the stability fields of *e.g.*, greenalite, minnesotaite and stilpnomelane, the estimated burial temperatures cannot be evaluated independently in any quantitative fashion, by the use of the iron-formation assemblages. One can only say that they appear, on the basis of textures and mineralogy, to be of late diagenetic to very low metamorphic grade origin.

## Acknowledgments

Research on this project was begun during a Guggenheim Memorial Fellowship awarded C.K. for 1978. Diamond drill cores were made available by the Hamersley Exploration Pty. Limited in Wittenoom, Western Australia. We thank Messrs. Bill Burns and John Evans of the Hamersley Exploration Pty. Ltd. for their advice and aid in the selection of materials. The Division of Mineralogy of the Commonwealth Scientific and Industrial Research Organization (CSIRO) in Perth, Western Australia, provided C.K. with office and laboratory space as well as field vehicles. C.K. is grateful to Messrs. W. E. Ewers and A. J. Gaskin of the CSIRO for their hospitality and support during his six months stay in Western Australia. Laboratory research was made possible by NSF grant EAR-76-11740 to C.K. The electron microprobe used in this study was obtained by joint funding from NSF grant GA-37109 (to C.K.) and the Indiana University Foundation. We thank Messrs. W. H. Moran, R. T. Hill, and G. R. Ringer for drafting and photography of the illustrations; Mrs. Thea Brown for the typing of the manuscript; and W. E. Ewers, H. L. James, R. C. Morris, A. F. Trendall, and R. E. Smith for critical and constructive reviews of the manuscript.

## References

Becker, R. H. and Clayton, R. N. (1976) Oxygen isotope study of a Precambrian banded iron-formation. Hamersley Range, Western Australia. Geochimica et Cosmochimica Acta, 40, 1153–1165.

Bricker, O. P., Nesbitt, H. W. and Gunter, W. D. (1973) The stability of talc. American Mineralogist, 58, 64–72.

Ernst, W. G. (1962) Synthesis, stability relations, and occurrence of riebeckite and riebeckite-arfvedsonite solid solutions. Journal of Geology, 70, 689–736.

Ewers, W. E. and Morris, R. C. (1980) Chemical and mineralogical data from the uppermost section of the upper BIF member of the Marra Mamba Iron Formation. CSIRO, Institute of Earth Resources, Division of Mineralogy, Report no. FP23.

Floran, R. J. and Papike, J. J. (1975) Petrology of the low-grade rocks of the Gunflint Iron Formation, Ontario-Minnesota. Geological Society of America, Bulletin 86, 1169–1190.

French, B. M. (1968) Progressive contact metamorphism of the Biwabik Iron Formation, Mesabi Range, Minnesota. Minnesota Geological Survey, Bulletin 45.

Gole, M. J. (1980) Mineralogy and petrology of very-low-metamorphic grade Archean banded iron-formations, Weld Range, Western Australia. American Mineralogist, 65, 8–25.

Gole, M. J. and Klein, C. (1981) Banded iron-formations through much of Precambrian time. Journal of Geology, 89, 169–183.

Haase, C. S. (1979) Metamorphic petrology of the Negaunee Iron Formation, Marquette district, Northern Michigan. Ph.D. thesis, Indiana University.

James, H. L. (1954) Sedimentary facies of iron-formation. Economic Geology, 49, 236–281.

James, H. L. (1955) Regional metamorphism in the Precambrian of northern Michigan, 66, 1455–1488.

Klein, C. (1974) Greenalite, stilpnomelane, minnesotaite, crocidolite and carbonates in a very low grade metamorphic Precambrian iron-formation. Canadian Mineralogist, 12, 475–498.

Klein, C. (1978) Regional metamorphism of Proterozoic iron-formation, Labrador Trough, Canada. American Mineralogist, 63, 898–912.

Klein, C. and Fink, R. P. (1976) Petrology of the Sokoman Iron Formation in the Howells River area, at the western edge of the Labrador Trough. Economic Geology, 71, 453–487.

Klein, C. and Bricker, O. P. (1977) Some aspects of the sedimentary and diagenetic environment of Proterozoic banded iron-formation. Economic Geology, 72, 1457–1470.

Kriewaldt, M. J. B. and Ryan, G. R. (1967) Pyramid, Western Australia: Western Australia Geological Survey 1:250,000, Geological Series Explanatory Notes.

Lesher, C. M. (1978) Mineralogy and petrology of the Sokoman Iron Formation near Ardua Lake, Quebec. Canadian Journal of Earth Sciences, 15, 480–500.

MacLeod, W. N. (1966) The Geology and iron deposits of the Hamersley Range area, Western Australia. Geological Survey of Western Australia, Bulletin 117.

Milton, C. and Eugster, H. P. (1959) Mineral assemblages of the Green River Formation. In P. H. Abelson, Ed., Researches in Geochemistry, p. 118–151. John Wiley and Sons, New York.

Papike, J. J., K. L. Cameron, and Baldwin, K. (1974) Amphiboles and pyroxenes: characterization of *other* than quadrilateral components and estimates of ferric iron from microprobe data. Geological Society of America, Abstracts with Programs, 1053.

Smith, R. E. (1980) Recognizing the paths of metamorphic/metasomatic fluids in a basic volcanic pile, Hamersley Basin, Western Australia. International Geologic Congress, Paris, Abstract Volume 1, 93.

Smith, R. E., Pedrix, J. L. and Parks, T. C. (1981) Burial metamorphism in the Hamersley Basin, Western Australia. Journal of Petrology, in press.

Trendall, A. F. (1973) Varve cycles in the Weeli Wolli Formation of the Precambrian Hamersley Group, Western Australia. Economic Geology, 68, 1089–1098.

Trendall, A. F. and Blockley, J. G. (1970) The iron-formations of the Precambrian Hamersley Group, Western Australia. Geological Survey of Western Australia, Bulletin 119.

Zajac, I. S. (1974) The stratigraphy and mineralogy of the Sokoman Formation in the Knob Lake area, Quebec and Newfoundland. Geological Survey of Canada Bulletin 220.

*Manuscript received, October 3, 1980;*
*accepted for publication, January 19, 1981.*